

# Hydrodynamics of Neutron Star Mergers

Joshua A. Faber and Frederic A. Rasio

*Department of Physics, M.I.T., 77 Massachusetts Ave., Cambridge, MA 02139*

**Abstract.** The final burst of gravitational radiation emitted by coalescing binary neutron stars carries direct information about the neutron star fluid, and, in particular, about the equation of state of nuclear matter at extreme densities. The final merger may also be accompanied by a detectable electromagnetic signal, such as a gamma-ray burst. In this paper, we summarize the results of theoretical work done over the past decade that has led to a detailed understanding of this hydrodynamic merger process for two neutron stars, and we discuss the prospects for the detection and physical interpretation of the gravity wave signals by ground-based interferometers such as LIGO. We also present results from our latest post-Newtonian SPH calculations of binary neutron star coalescence, using up to  $10^6$  SPH particles to compute with higher spatial resolution than ever before the merger of an initially irrotational system. We discuss the detectability of our calculated gravity wave signals based on power spectra.

## INTRODUCTION

Coalescing binary neutron stars (NS) are among the most promising sources of gravitational radiation that should be detectable by future generations of gravity wave detectors. LIGO, VIRGO, GEO, and TAMA may ultimately not only serve to test the predictions of the theory of general relativity (GR), but could also yield important information on the interior structure of neutron stars, which cannot be obtained directly in any other way.

Compact binary orbits decay through energy losses to gravitational radiation. So long as the separation between the two NS is large, the binary inspiral is well described by a point-mass treatment, modified to take into account finite-size and relativistic effects, which act only as small corrections. At the end of the inspiral, however, the process is inherently hydrodynamic in nature. Large tidal interactions can drive the system into dynamical instability, at which point a quasi-equilibrium treatment of the binary breaks down, and a numerical treatment is required to accurately model the system.

Essentially all recent calculations agree on the basic picture that emerges for the final coalescence (see [1] and [2] for a complete list of references). As the dynamical stability limit is approached, typically at separations of  $r = 3 - 4R_{NS}$ , depending on the choice of parameters, the NS undergo a rapid radial plunge and merge in

no more than a few rotation periods, much more quickly than would be predicted by a point-mass formula. In many cases, especially for binaries assumed to be initially synchronized, mass shedding sets in immediately after the stars first make contact. Material with a high specific angular momentum located in the outer regions of each NS is shed through the outer Lagrange points of the system, forming spiral arms that encircle the merger remnant left in the center as the NS cores merge. Eventually, the spiral arms also merge into a nearly axisymmetric torus around the dense inner core. For a stiff equation of state (EOS), a core with a significant ellipsoidal (triaxial) deformation can be maintained, and the configuration keeps radiating gravity waves well after the merger is completed. Softer EOS cannot support such a configuration stably, and any remnant produced will relax on a dynamical timescale toward a spheroidal (axisymmetric) configuration, which produces a negligible amount of gravity waves.

The previous statements assume that the merger remnant formed is stable against gravitational collapse to a black hole. Unfortunately, Newtonian calculations are incapable of demonstrating such an effect. Post-Newtonian (PN) simulations can produce configurations that are unstable against collapse, but they are inherently unreliable because in conditions of strong gravity the basic assumptions of the PN expansion break down. Early full GR calculations indicate that merger remnants may very well be stable against collapse, so long as the EOS is assumed to be stiff enough [3]. The mass of the remnant should be nearly twice the mass of a single NS, which is generally taken to be  $M_{NS} \approx 1.4 - 1.5 M_{\odot}$ , and thus well over the maximum mass for a single, nonrotating NS. However, the remnants formed in binary coalescence are very rapidly and differentially rotating, which can increase the maximum stable mass to a much larger value [4,5].

## BINARY NS COALESCENCE CALCULATIONS

Nakamura and collaborators [6,7] were the first group to perform 3-D hydrodynamic calculations of binary NS coalescence, using an Eulerian grid-based code. Rasio and Shapiro [8] used the Lagrangian SPH (Smoothed Particle Hydrodynamics) method to calculate gravitational wave forms from binary coalescence events. Calculations performed since, using both Eulerian methods [10–14] and SPH [15–18] have focused on several aspects of the problem, including the effects of different initial spins, mass ratios, NS EOS, and NS masses. Some groups have incorporated treatments of the nuclear physics involved in the merger [12–14,16–18] in order to study coalescing NS binaries as possible gamma-ray burst sources, and as possible birthplaces for r-process elements.

Much of the early work on coalescing NS binaries assumed Newtonian gravity for simplicity. Later studies added a treatment of the radiation reaction, which is responsible for driving the system towards coalescence, either by adding a frictional drag term to model point-mass inspiral [15–18], or by an exact PN treatment [12–14]. In essence, 2.5PN radiation reaction terms (which scale like  $1/c^5$ )

are added onto a Newtonian framework, but all lower-order non-dissipative terms are ignored. Unlike adding a frictional drag term which dissipates energy according to the point-mass prediction, the lowest-order treatment of the radiation reaction allows for its effects to be included throughout the entire calculation, including the period after the merger remnant has formed. Unfortunately, however, Newtonian gravity is known to be a poor description of the physical problem at hand. Even NS with stiff EOS generate strong gravitational fields. During the final moments before merger, the velocities found in the system also become relativistic. Thus, the hydrodynamics of the actual coalescence can only be calculated properly by taking into account GR effects.

The Newtonian limit also fails to describe accurately the onset of dynamical instability. PN effects combine nonlinearly with finite-size fluid effects and this can dramatically increase the critical binary separation (and thus lower the frequency) at which dynamical instability sets in. Indeed, the quasi-equilibrium description applies so long as

$$\left(\frac{dE}{dr}\right)_{equil} > \left(\frac{dE}{dt}\right)_{GW} \left(\frac{dr}{dt}\right)_{infall}^{-1}, \quad (1)$$

where  $E_{equil}(r)$  is the energy of an equilibrium binary configuration at a given separation  $r$ . Equilibrium sequences have been calculated for both synchronized and irrotational binaries in Newtonian gravity [19], PN gravity [20], and recently in full GR [21,22] (see also Baumgarte, in this volume). It is generally found that the energy of NS binary configurations reaches a minimum at some critical separation, defining the innermost stable circular orbit (ISCO). Relativistic terms move the ISCO to larger separations, and also reduce the slope of the energy curve just outside the ISCO. Thus, the assumption of quasi-equilibrium, which is used to set up the initial configuration of the binary system, breaks down at a much larger separation than a Newtonian calculation would predict. In addition, NS binaries will already have developed significant infall velocities as they pass through the ISCO calculated for systems in strict equilibrium.

Several groups have been working on full GR calculations of binary NS mergers, but only preliminary results have been reported so far [23]. Proving to be particularly difficult is the extraction of wave forms from the boundaries of large 3-D grids, since extending the grids into the true wave zone would be too expensive computationally. The middle ground between the Newtonian treatments and full GR lies in PN hydrodynamic calculations of binary mergers. The authors [1,24], as well as Ayal et al. [25], have constructed a PN SPH code, described below, for calculating binary mergers. While it too serves only as an approximation to the proper physics which must go into a realistic calculation, the results do provide insight into the relativistic effects that simple Newtonian intuition fails to handle correctly. Additionally, they should serve as valuable checks for future full GR calculations, lending confidence to wave form predictions, and indicating to some degree the difference between real relativistic effects and numerical instabilities.

## POST-NEWTONIAN SPH

Our Post-Newtonian calculations use a formalism adapted from that of Blanchet, Damour, and Schaefer [26]. It includes all first-order (1PN) terms of GR, as well as the lowest-order radiation reaction terms (2.5PN). The latter are important because they provide the energy dissipation mechanism which drives the binary system toward dynamical instability and coalescence. Calculating various PN quantities requires the solution of seven additional Poisson equations for 1PN terms and an additional Poisson equation for the radiation reaction, all of which have compact support and thus can be solved by similar methods as the Newtonian gravitational potential. All hydrodynamic quantities in the formalism have been converted from a grid-based Eulerian approach to a particle-based Lagrangian approach, where particles represent distributions of matter in space defined by a spherically symmetric smoothing kernel (rather than point-like objects). Pressure forces and other interactions between particles are handled by summing over neighboring particles. Poisson equations are solved by translating particle-based source term quantities onto a grid, and solving via FFT-based convolution methods [24].

Unfortunately, the consistent use of physically realistic NS parameters is impossible in this PN formalism. The compactness of a NS is given by

$$\frac{GM}{Rc^2} = 0.20 \left( \frac{M}{1.5M_{\odot}} \right) \left( \frac{10 \text{ km}}{R} \right), \quad (2)$$

and is typically assumed to fall near  $GM/Rc^2 \approx 0.15$  for a reasonable choice of EOS. Since several of the coefficients of the 1PN terms can be quite large, especially for stiff EOS, we find that in many cases the 1PN corrections are larger than the Newtonian terms. Thus, we adapt the formalism, reducing the magnitude of the 1PN corrections by a factor of three (in effect decreasing the mass of the NS to  $M_{1PN} = 0.5M_{\odot}$ ), but treating all the radiation reaction terms, of significantly smaller magnitude, at full strength. In essence, we employ a different speed of light for 1PN and 2.5PN terms. By comparison with result including radiation reaction but no 1PN terms whatsoever, we believe we can extrapolate in a qualitative sense toward the proper physically realistic case. By comparison, self-consistent PN calculations performed for NS with artificially small masses [7,25] have the advantage that they can be directly compared to full GR calculations, for which there can be no separation of relativistic terms into separate orders. Unfortunately, these calculations also suffer from a drastic and completely artificial reduction of the radiation reaction effects, which scale like  $M^{2.5}$ . This produces a significant delay in the onset of dynamical instability past the point where it would be encountered for a physical set of parameters, and can lead to a qualitatively incorrect description of the subsequent merger.

## IRROTATIONAL BINARY COALESCENCE

Our most detailed calculation performed to date uses  $N = 500,000$  particles per NS, corresponding to the highest spatial resolution ever for a binary coalescence calculation. The spatial resolution (smoothing length) achieved in the central regions of the stars is  $h \approx 0.03R_{NS}$ . The calculation was performed using an irrotational initial condition. This is generally thought to be the most realistic case since the viscous tidal locking timescale for two NS is expected to be considerably longer than the inspiral timescale [27]. Corotating (tidally locked) systems are motionless in a frame corotating with the binary, which allows for the use of relaxation techniques that can give a very accurate equilibrium initial condition (thus nearly completely eliminating spurious oscillations around equilibrium during the early phases of the dynamical evolution). Instead, for our irrotational calculation, we model the initial density and velocity profile of the NS as tidally stretched ellipsoids, with parameters drawn from the PN equilibrium calculations of Lombardi, Rasio, and Shapiro [20].

Since all NS in relativistic binary systems are expected to have masses that lie within a very narrow range [28], our calculation uses equal-mass NS. As the NS EOS is still poorly constrained, we choose a simple  $\Gamma = 3$  polytropic EOS, i.e., the pressure is given in terms of the rest-mass density by  $P = k\rho_*^3$ . Stiff EOS, such as this one, are capable of maintaining a long-lived ellipsoidal deformation after the binary merger, with a gravity wave signal that persists on a timescale much longer than the merger timescale [9].

Particle plots showing the evolution of the equal-mass irrotational binary system are shown in Fig. 1. We see that immediately prior to merger a large tidal lag angle develops. The inner edge of each NS leads the axis connecting the centers of mass of the binary components, and the outer regions lag behind. This effect is seen even in Newtonian simulations, but is greatly enhanced by the addition of 1PN correction terms. When first contact is made, a long vortex sheet forms at the interface between the two stars. Unlike the case of synchronized binaries, we do not see significant mass shedding from the outer Lagrange points of the system. The rotational speed of particles on the outer half of each NS is reduced in the irrotational case with respect to the synchronized case, and such particles remain bound and form the outer regions of the eventual merger remnant. At  $t = 25$  we do see some hint of mass shedding, but not via the mechanism described above. Particles which have travelled the length of the vortex sheet and retained significant velocities end up being shed from the leading edge of the vortex sheet. It is important to note, though, that the amount of mass shed is extremely small, much less than 1% of the total mass, and that the velocities of the particles ejected are not sufficient to escape the gravitational potential of the remnant. We thus expect them to form an extremely tenuous halo around the central core. At late times, we see the formation of a remnant containing essentially all the mass that was originally present in the system. As we are using a stiff EOS, the ellipsoidal deformation of the remnant is relatively large, and persists for late times after the

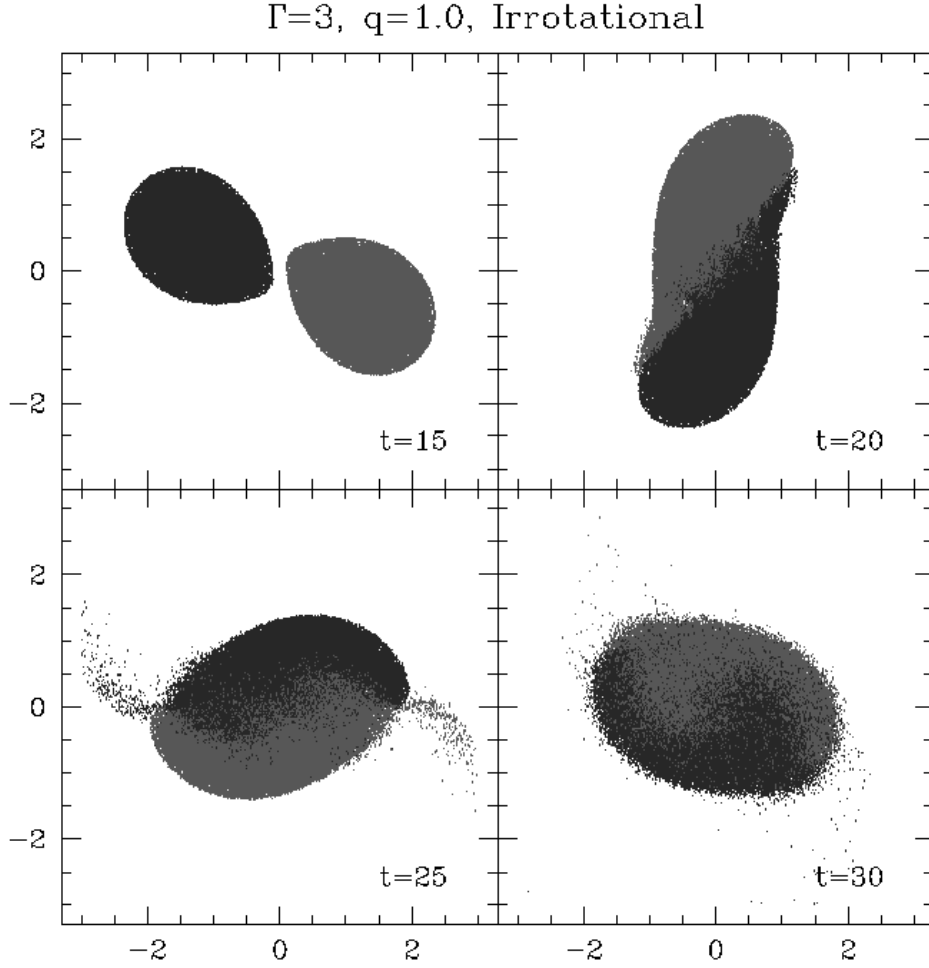


**FIGURE 1.** Final merger of two identical  $\Gamma = 3$  polytropes with an irrotational initial condition. SPH particles are projected onto the equatorial plane of the binary. The orbital rotation is counterclockwise. Spatial coordinates are given in units of the NS radius  $R$ . Times are given in units of the dynamical timescale of the system, which here is  $t_D = 0.07\text{ms} = 1$ . The orbital rotation is in the counterclockwise direction.

merger.

Density contours and velocity profiles in the equatorial plane of the binary are shown in Fig. 2. Velocities are shown in a frame corotating with the material. We see that the initially counterstreaming surfaces of the NS produce a vortex sheet, which is Kelvin-Helmholtz unstable. Large vortices develop along the surface of contact, both in the center of the forming merger remnant and also at a separation which seems to be roughly consistent with the misalignment of the leading edges of each NS, or about  $r = 0.5R$ . As the merger proceeds, we see that the vortices re-

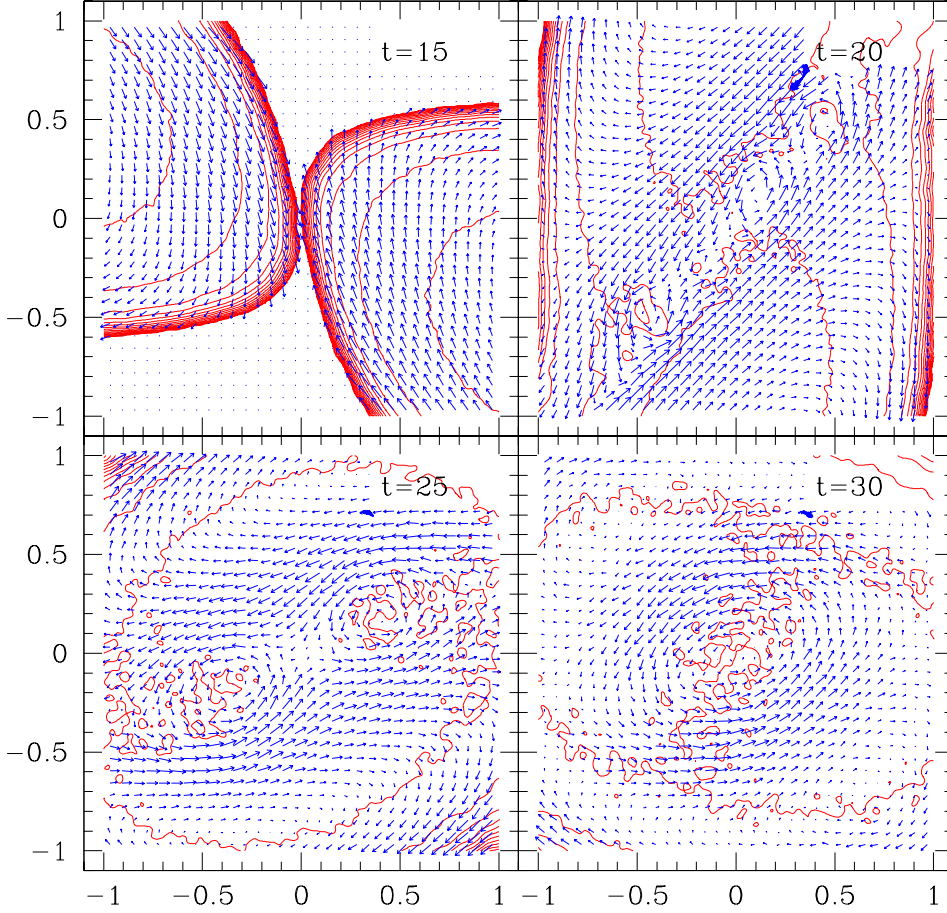


**FIGURE 2.** Density contours and velocities along the equatorial plane in the corotating frame of the binary, for the same times as in Fig. 1.

main coherent from  $t = 20 - 25$ , mixing material which was originally located along the inner parts of each NS. All the while, the cores of the respective NS continue to inspiral toward the center of the merger remnant, until by  $t = 30$  they have formed a single core, the vortices having merged together. This produces a characteristic differentially rotating pattern, with the center of the remnant spinning approximately twice as fast as the outer regions.

## GRAVITY WAVE SIGNALS AND SPECTRA

We calculate the gravity wave signal for our mergers in the quadrupole approximation. The gravity wave strain  $h$  seen by an observer located a distance  $d$  from

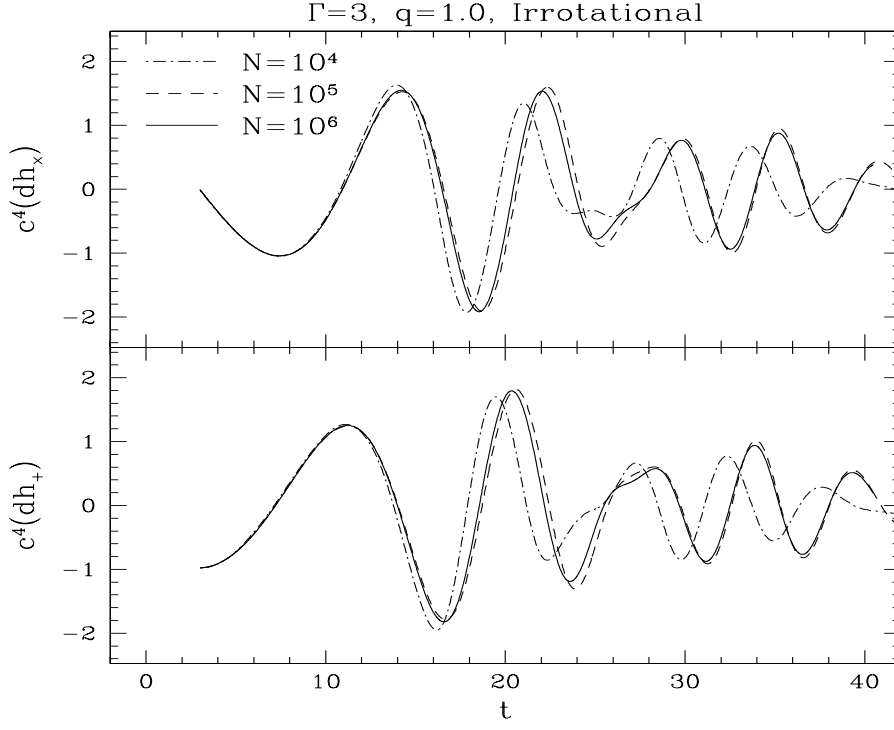


**FIGURE 3.** Gravity wave signals calculated for coalescences with the same initial parameters but different numerical resolutions. The solid, dashed, and dot-dashed lines correspond to runs with  $10^6$ ,  $10^5$ , and  $10^4$  SPH particles, respectively.

the center of mass of the system along the rotation axis is given for the two polarizations by

$$c^4(dh_+) = \ddot{Q}_{xx} - \ddot{Q}_{yy} \quad (3)$$

$$c^4(dh_\times) = 2\ddot{Q}_{xy} \quad (4)$$

where  $\ddot{Q}$ , the second time derivative of the quadrupole moment tensor, is given in SPH terms by

$$\ddot{Q}_{ij} = \sum_b m_b (v_i^{(b)} v_j^{(b)} + x_i^{(b)} \dot{v}_j^{(b)} + x_j^{(b)} \dot{v}_i^{(b)}) \quad (5)$$

where the summation is taken over all particles in the calculation.

In Fig. 3, we show the gravity wave signals in both polarizations for the irrotational run described above, as well as for runs with  $N = 50,000$  particles and  $N = 5,000$  particles per NS. It is immediately apparent that the lowest resolution run shows significant discrepancies from the other two, which agree with each other quite well over the entire time history of the merger. This is a welcome result, given that the vortex sheet appearing at the contact surface is Kelvin-Helmholtz

unstable on all wavelengths, including those much smaller than our numerical resolution. Calculations performed at different resolutions do show subtle differences in the exact location and size of the vortices. It is important to note, however, that it is the outer regions of the star, at lower density, that supply material to the vortex sheet. The high density cores of the two NS inspiral during the entire process, and provide the dominant component of the quadrupole moment and thus the gravity wave signal. The path traced out by the NS cores depends sensitively on gravitational forces and properties of the fluid, such as the EOS, but proves to be remarkably insensitive to the details of the flow in the “turbulent” boundary region. The conclusion to be drawn is that numerical convergence for a given set of initial conditions and physical assumptions is possible without requiring excessive computational resources, even for this difficult problem involving small-scale instabilities.

Because the gravity wave signals expected to be seen from binary NS mergers are extremely close to the sensitivity limits of ground-based interferometers, it is important to identify which features in the power spectrum of the gravitational radiation will yield the most information on the physical parameters of NS. Following the method of Zhuge et al. [15], we compute the gravity wave power spectrum per unit frequency interval as

$$\frac{dE_{GW}}{df} = \frac{c^3}{G} \frac{\pi}{2} (4\pi r^2) f^2 \langle |\tilde{h}_+(f)|^2 + |\tilde{h}_\times(f)|^2 \rangle. \quad (6)$$

Before calculating the power spectra from our simulations, we add a component representing a point-mass inspiral matched to the beginning of our hydrodynamic merger wave form. This produces a spectrum with  $dE/df \propto f^{1/3}$  for point-mass inspiral at low frequencies. In essence, what we measure here is the number of orbits spent around a given frequency, weighted by the amplitude of the emission. We identify three frequencies of special interest. The frequency at which dynamical instability sets in is labeled  $f_{dyn}$ . The frequency at the peak of the gravity wave luminosity is labeled  $f_{peak}$ . Last, the characteristic frequency of gravity wave emission for the merger remnant at late times in the calculation is labeled  $f_{osc}$ .

In Fig. 4, we show the gravity wave power spectrum for a Newtonian calculation with a synchronized initial condition, which includes radiation reaction effects but contains no 1PN terms. At low frequencies, we see the power-law behavior from the point-mass inspiral, with no contribution whatsoever from our calculated signal. At the dynamical instability frequency, we see a slight decrease in the gravity wave power, since the rapid plunge causes the binary to sweep up faster through a range of characteristic frequencies. The gravity wave power shows a plateau near the peak emission frequency, when the effects of the rapid infall are balanced by the large increase in gravity wave amplitude. At higher frequencies, there is another slight dip in emission, followed by a sharp peak marking the oscillation frequency of the merger remnant. With more careful handling of the late-time behavior of the system, we expect the peak to remain prominent, but our calculation most likely overemphasizes the coherence of the signal.

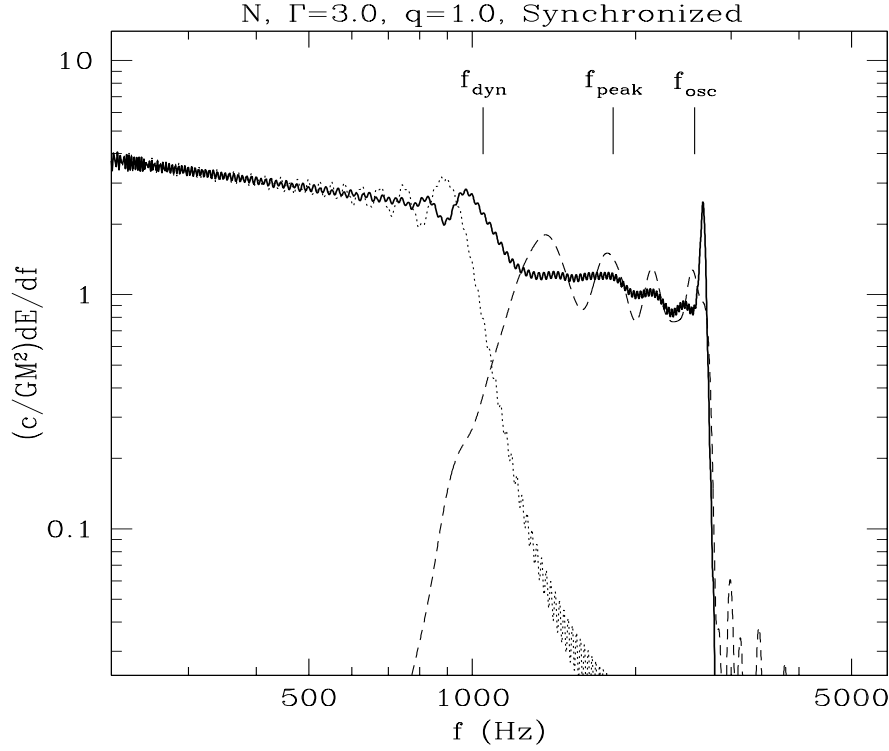


**FIGURE 4.** Power spectrum calculated from a Newtonian coalescence calculation. The dotted and dashed lines represent the contributions of the point-mass inspiral and our calculated gravity wave signal for the hydrodynamic merger, respectively. The solid line represents the total power.

A strikingly different power spectrum is obtained from our Post-Newtonian, irrotational merger, as shown in Fig. 5. The most significant difference between the two concerns the limit of dynamical instability. Newtonian gravity is strengthened by the addition of relativistic effects, which moves the dynamical stability limit to larger separations (and thus smaller frequencies). Additionally, the final plunge of the two NS is much faster, which significantly reduces the power in the region between  $f_{dyn}$  and  $f_{peak}$ . At  $f_{peak}$ , the power is smaller than in the Newtonian case, but the signal is much more sharply defined. Similarly, the oscillation of the remnant at late times leaves a well defined imprint on the power spectrum, but the amplitude of the peak is approximately an order of magnitude lower than what is found in a Newtonian calculation.

The frequencies of the two peaks seen in the spectrum, representing peak emission and the remnant oscillations, do give a strong clue to the nature of the NS EOS. While the frequency of peak oscillation is essentially the same in all our simulations, the width of the peak is seen to be strongly dependent on the EOS. The softer  $\Gamma = 2$  EOS shows a broad peak of emission in the frequency range  $f \sim 1500 - 3000$  Hz, whereas the stiffer  $\Gamma = 3$  EOS calculations have a peak much more focused around  $f = 1800 - 2200$  Hz, regardless of the initial spins. The remnant oscillations break

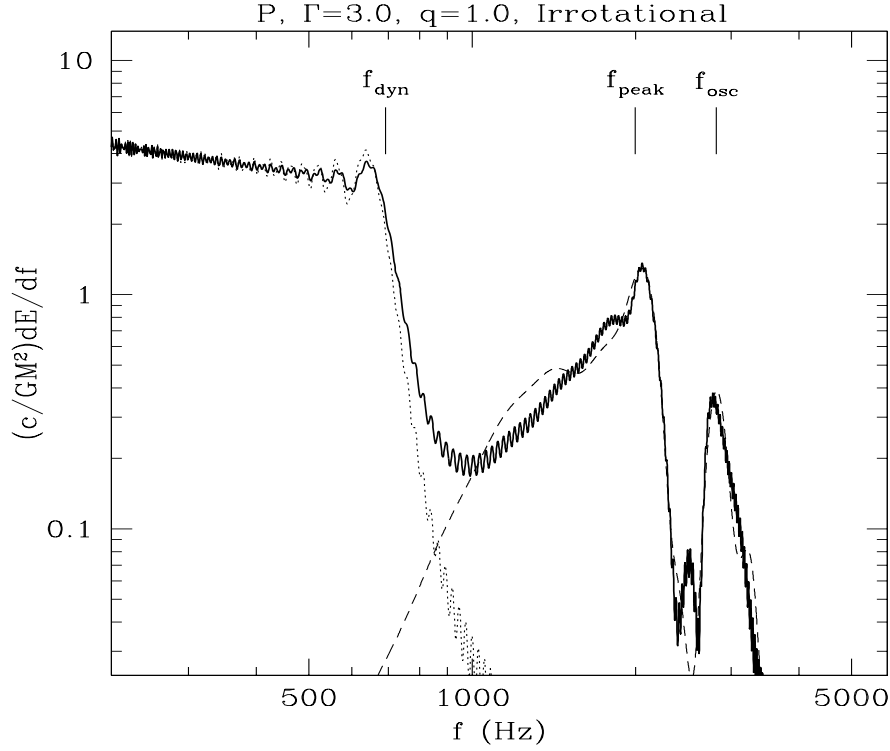


**FIGURE 5.** Power spectrum from a Post-Newtonian coalescence calculation. Conventions are as in the previous figure.

this degeneracy. The oscillation frequency for the irrotational run is almost 15% less than that of the synchronized run with the same choice of EOS. The stiffer EOS also results in a more rapid oscillation than the softer one, although the frequencies are relatively similar.

In general, several trends can be recognized regarding the strength of gravity wave emission from NS binary coalescence. The large dip at the dynamical instability limit is a general feature of PN calculations, regardless of the choice of initial spins or the EOS. It should be regarded as a consequence of the stronger gravity present in the PN systems. Additionally, PN simulations generally show similar amplitudes to their Newtonian counterparts near the characteristic frequency of peak emission, but significantly less power at higher frequencies, since the effect of strong gravity seems to be a quenching of gravity wave emission after the initial peak. Soft EOS generally show greatly reduced gravity wave emission at high frequencies, since they cannot support a stable, radiating, ellipsoidal configuration, and on relatively short timescales will produce a nearly spheroidal, non-radiating remnant. Finally, for binary systems with unequal-mass components, the magnitude of the gravity wave emission is strongly correlated with the mass ratio  $q$  [1,9]. Because the primary in such systems generally remains relatively undisturbed, whereas the secondary is tidally disrupted and accreted onto the primary, a large component of

the matter essentially does not contribute to the gravity wave signal. Thus, even if NS masses do not typically lie within a narrow range, there should be a strong bias observationally toward detection of nearly equal-mass systems.

## ACKNOWLEDGMENTS

This work was supported in part by NSF Grants AST-9618116 and PHY-0070918 and NASA ATP Grant NAG5-8460. F.A.R. was supported in part by an Alfred P. Sloan Research Fellowship. The computations were supported by the National Computational Science Alliance under grant AST980014N and utilized the NCSA SGI/CRAY Origin2000.

## REFERENCES

1. Faber, J.A., Rasio, F.A., and Manor, J.B., *Phys. Rev. D*, accepted, gr-qc/9912097.
2. Rasio, F.A., and Shapiro, S.L., *Class. Quant. Grav.* **16**, R1-R29 (1999).
3. Shibata, M., and Uryu, K., *Phys. Rev. D* **61**, 064001 (2000).
4. Baumgarte, T.W., Shapiro, S.L., and Shibata, M., *Astrophys. J. Lett.* **528** L29-L32 (2000).
5. Rasio, F.A., “The Final Fate of Coalescing Binary Neutron Stars: Collapse to a Black Hole?” to appear in *Black Holes in Binaries and Galactic Nuclei*, edited by L. Kaper, E.P.J. van den Heuvel, and P.A. Woudt, ESO Press.
6. Oohara, K., and Nakamura, T., *Prog. Theor. Phys.* **82**, 535-554 (1989); *ibid.* **83**, 906-940 (1990); Nakamura, T. and Oohara, K., *ibid.* **82**, 1066-1083 (1989); *ibid.* **86**, 73-88 (1991).
7. Shibata, M., Oohara, K., and Nakamura, T., *Prog. Theor. Phys.* **88**, 1079-1095 (1992); *ibid.* **89**, 809-819 (1993).
8. Rasio, F.A., and Shapiro, S.L., *Astrophys. J.* **401**, 226-245 (1992); *ibid.* **438**, 887-903 (1995).
9. Rasio, F.A., and Shapiro, S.L., *Astrophys. J.* **432**, 242-261 (1994).
10. New, K.C.B., and Tohline, J.E., *Astrophys. J.* **490**, 311-327 (1997).
11. Swesty, F.D., Wang, E.Y.M., and Calder, A.C., *Astrophys. J.* **541**, 937-958 (2000).
12. Ruffert, M., Janka, H.-Th., and Schäfer, G., *Astron. Astrophys.* **311**, 532-566 (1996).
13. Ruffert, M., Janka, H.-Th., Takahashi, K., and Schäfer, G., *Astron. Astrophys.* **319**, 122-153 (1997).
14. Ruffert, M., Rampp, M., and Janka, H.-Th., *Astron. Astrophys.* **321**, 991-1006 (1997).
15. Zhuge, X., Centrella, J., and McMillan, S., *Phys. Rev. D* **50**, 6247-6261 (1994); *ibid.* **54**, 7261-7277 (1996).
16. Davies, M.B. et al., *Astrophys. J.* **431**, 742-753 (1994).
17. Rosswog, S. et al., *Astron. Astrophys.* **341**, 499-526 (1999).
18. Rosswog, S. et al., *Astron. Astrophys.* **360**, 171-184 (2000).

19. Lai, D., Rasio, F.A., and Shapiro, S.L., *Astrophys. J. Lett.* **406**, L63-L66 (1993); *Astrophys. J. Suppl.* **88**, 205-252 (1993); *Astrophys. J.* **420**, 811-829 (1994); *ibid.* **423**, 344-370 (1994); *ibid.* **437**, 742-769 (1994).
20. Lombardi, J.C., Rasio, F.A., and Shapiro, S.L., *Phys. Rev. D* **56**, 3416-3438 (1997).
21. Baumgarte, T.W. et al., *Phys. Rev. Lett.* **79** 1182-1185 (1997).
22. Bonazzola, S., Gourgoulhon, E., and Marck, J.-A., *Phys. Rev. Lett.* **82** 892-895 (1999).
23. Baumgarte, T.W., Hughes, S.A., and Shapiro, S.L., *Phys. Rev. D.* **60**, 087501 (1999); Shibata, M., *Phys. Rev. D* **60**, 104052 (1999).
24. Faber, J.A. and Rasio, F.A., *Phys Rev. D* **62**, 064012 (2000).
25. Ayal, S. et al., *Astrophys. J.*, accepted, astro-ph/9910154.
26. Blanchet, L., Damour, T., and Schäfer, G., *Mon. Not. Roy. Astron. Soc.* **242**, 289-305 (1990).
27. Bildsten, L., and Cutler, C., *Astrophys. J.* **400**, 175-180 (1992).
28. Thorsett, S.E., and Chakrabarty, D., *Astrophys. J.* **512**, 288-299 (1999).